Chapter 1

Failure Assessment of Piezoelectric Actuators and Sensors for Increased Reliability of SHM Systems

Inka Mueller and Claus-Peter Fritzen

Additional information is available at the end of the chapter

http://dx.doi.org/10.5772/intechopen.77298

Abstract

In the chain from sensing to information extraction, there are many traps where errors can occur, which might lead to false alarms and therefore leave us with the impression of an unreliable system. In this chapter, we deal with the important first element of the chain, the sensor, which can undergo various faults and defects during its lifetime. Especially for the use of acousto-ultrasonic (AU)-based methods or the electro-mechanical impedance (EMI) method, piezoelectric transducers are frequently used. Subsequent steps within the chain of SHM rely on the quality and reliability of these measurements. An overview is given on the usage of piezoelectric transducers within SHM systems, their electro-mechanical coupling and its modeling as well as frequent faults of these devices and methods on how to inspect them and diagnose defects. The authors show the effects of different transducer faults on the excited wave field, used for AU. It is shown how a sensor fault can be detected before the SHM system indicates a (false) alarm. With the help of application scenarios—including temperature variations—the advantages and disadvantages of the introduced methods of transducer inspection are presented, enabling an increased reliability of SHM systems.

Keywords: piezoelectric transducers, piezoelectric wafer active sensors, faults, defects, electro-mechanical impedance, acousto-ultrasonics, guided waves, lamb waves, structural health monitoring, system reliability

1. Introduction

Aspects of reliability play a major role for the development of structural health monitoring (SHM) systems in working industrial applications. This reliability has to be ensured for all

steps of the SHM process, which are, according to Farrar and Worden, (1) operational evaluation, (2) data acquisition, (3) feature selection and (4) statistical modeling for feature discrimination [1]. Within this chapter, the second step "data acquisition" is focused. It is closely linked to the third step, which aims at extracting the damage relevant information from the measured data via data analysis. Within the toolbox of methods used for SHM, the two groups vibration-based methods and wave-based methods have emerged. Vibration-based methods are based on the fact that modal parameters like eigenfrequencies, mode shapes and modal damping are functions of physical properties like the distribution of stiffness or of mass. In case of damage, physical properties are changed, leading to a change of the modal parameters, which are monitored by vibration-based SHM systems. Moreover, we can go to the higher frequency range and evaluate the time data directly. For their monitoring, excitation is necessary, which is often achieved by using ambient excitation, e.g., cars crossing a bridge to be monitored. Wave-based SHM methods either use the fact that a damage, e.g., cracks or breaking fibers within a composite component, will result in an emitted acoustic signal or use the fact that a wave will interfere with a possible damage. For the first, the acoustic signal will travel through the component and be detected by members within a net of listening sensors. Data evaluation will identify these single events and might locate the crack's position via triangulation. While this method is a passive method, the wave-based acousto-ultrasonics method is characterized as an active method. A well-defined excitation is used, creating a wave, which travels through the structure, interferes with specific geometric features of the structure, like edges, thickness, changes but also damages and is sensed after these interferences, e.g., at a different point of the structure. When traveling through thin-walled plates or rods, waves often appear as guided waves. They are reflected, can convert into different modes or the transmitted part is changed by discontinuities, like damages. Therefore, a change of the evaluated signal is interpreted as an indicator for damage.

For all SHM systems, it has been shown that the influence of environmental and operational conditions cannot be neglected. If we ignore a change of temperature, it might be interpreted as damage or a temperature change might decrease or even reverse the effect of damage. Depending on the SHM method, different approaches to tackle especially temperature changes have been proposed. For methods using acousto-ultrasonics, in [2] an overview of different methods for the compensation of temperature changes is given and the use of the local temporal coherence to cope with the changes of temperature and effects of surface wetting is detailed. Similar to this approach, for methods based on the signature of the electro-mechanical impedance (EMI) spectrum, in [3], a correlation coefficient-based method is used, which compensates frequency and magnitude shifts, caused by temperature changes, while changes of the shape, caused by damages within the structure, are identified. This method is applicable if the effects of damage can be clearly separated from effects of temperature variation. This is not the case for all applications. Therefore, in [4, 5], a physics-based compensation of the influences of temperature changes is used for EMI and acousto-ultrasonics (AU)-based methods. The effort for this method is large, as the temperature dependence of all significant parameters has to be included within the model. Other efforts to compensate for varying environmental and operational conditions for signal-based techniques within wave- and

vibration-based SHM systems use statistical damage classification [6, 7] including, e.g., fuzzy classification [8], the use of neural networks [9] and self-organizing maps [10].

For vibration-based SHM systems, the used sensors are often based on well-approved measurement sensors, which have been used in the past for different purposes, measuring strain, acceleration or displacement. The special requirements of SHM systems regarding the continuous monitoring on-site over long periods are achievable and the measurement systems might include a self-check and transducer electronic data sheets (TEDS) to increase the reliability, e.g., ICP compatible accelerometers. Wave-based methods often use a distributed sensor network and the included sensors are just starting to enter more into commercial products, e.g., PICeramic P-876.SP1 and Acellent SMART Layer [11, 12]. This chapter focuses on the wave-based methods, which use piezoelectric transducers for data acquisition, including actuation and sensing purposes.

Using guided waves, an SHM system identifies damages via comparing signals from different states. While the current state which should be evaluated is always based on measurements, the reference state, often taken from the pristine structure, can either be based on measurement data or set up by physics-based models. Occasionally, the comparison is also based on assumptions like the linear material behavior of the system in pristine state. The different methods of feature selection and feature discrimination are not within the focus of this chapter, as there are a multitude of possibilities. Nevertheless, the consideration of reliability on these steps is highly important and is a major research area to enable certification processes, necessary for the use of SHM systems in industrial applications.

Focusing the inspection of sensors and its self-test, different approaches can be found. Simple systems check, if the sensor signal is different from zero. More advanced data-driven methods are based on hardware redundancy [13]. Typical faults are bias, complete failure, drifting and precision degradation, see [14], as well as gain, noise and constant with noise [13]. For networks of wireless sensor nodes, these methods are used to find faulty nodes to be able to either replace those nodes or simply remove them from the network, which is only possible with sufficient redundancy, see e.g., [15]. The use of hardware redundancy, which tests if the sensor signal fits the assumed signal, when only using all other sensors, has been used for SHM systems, too. In [16], a modal filtering approach is used, and [17] uses a PCA-model to represent the signal in a lower-dimensional space and compare it with the original signal. The effect of temperature change and structural damage is considered in [18] using the mutual information concept. All these methods use the measurement data for a mathematical procedure not based on physical quantities. While it is an advantage that no additional measurements are needed, this also leads to difficulties in distinguishing between structural damage and sensor fault, especially for the case of small defects and in widespread sensor network. Depending on the type of sensor, physics-based methods of self-diagnosis using additional measurements can be found. Ref. [19] describes the use of electrical impedance spectroscopy measurement to enable self-monitoring of semiconductor gas sensor systems. In [20], methods to enable a validation of the sensor functions under operational conditions are suggested, which include the use of a magnetostrictive coated fiber. For piezoelectric wafer active sensors (PWAS), self-diagnosis capabilities exist, which are mainly based on the transducers physics.

For these transducers, the typical classification into gain, drifting, and so on does not represent the effects of faulty PWAS. The importance of reliable sensor data cannot be overestimated to achieve a reliable output of an SHM system over long monitoring periods.

Within this chapter, a short overview on the usage of piezoelectric transducers within AU-based SHM systems, their electro-mechanical structure and its modeling is given in Section 2. The effects of different transducer faults on the generated wave field, used for AU, as well as on the electro-mechanical impedance spectrum are described in Section 3. Section 4 shows a variety of methods for transducer inspection including model-based and data-based methods with different requirements on the available knowledge about the system and material parameters. Using application scenarios—also including temperature variations—the advantages and disadvantages of the introduced methods of transducer inspection, enabling an increased reliability of SHM systems, are presented in Section 5.

2. Tasks of piezoelectric transducers

In many applications, piezoelectric material is used purely for actuating or sensing purposes. The use of PWAS for SHM purposes is mostly including both, the inverse and the direct piezoelectric effect. In general, the piezoelectric effect is not linear. Nevertheless, the effect can be modeled linearly in a certain strain range for most piezoelectric materials. Moreover, the temperature needs to stay well below the Curie point. The actuation (inverse piezoelectric effect) can be described by

$$D_i = d_{ikl} T_{kl} + \varepsilon_{ik}^{T} E_k \tag{1}$$

$$S_{ij} = s_{ijkl}^{E} T_{kl} + d_{kij} E_k \tag{2}$$

with stress T, strain S, elastic compliance s, dielectric constant ε, electric field E, dielectric displacement D, defined by charge Q per unit area A at given stress T, and piezoelectric constants d, linking dielectric displacement with stress as well as strain with electric field.

Although these equations already fully describe the direct and inverse piezoelectric effect, for sensing purposes (direct piezoelectric effect) the most familiar description uses g as piezoelectric voltage coefficient to connect stress with electric field.

$$E_i = -g_{ikl} T_{kl} + \beta_{ik}^{T} D_k \tag{3}$$

$$S_{ij} = s_{ijkl}^{D} T_{kl} + g_{kij} D_k \tag{4}$$

These equations can be simplified especially in their dimension, when using Voigt notation and assuming multiple symmetry in the piezoelectric materials as well as in the strain and stress tensors.

$$\begin{bmatrix} D_1 \\ D_2 \\ D_3 \end{bmatrix} = \begin{bmatrix} 0 & 0 & 0 & 0 & d_{15} & 0 \\ 0 & 0 & 0 & d_{15} & 0 & 0 \\ d_{31} & d_{31} & d_{33} & 0 & 0 & 0 \end{bmatrix} \begin{bmatrix} T_{11} \\ T_{22} \\ T_{33} \\ T_{23} \\ T_{13} \\ T_{12} \end{bmatrix} + \begin{bmatrix} \varepsilon_{11}^T & 0 & 0 \\ 0 & \varepsilon_{11}^T & 0 \\ 0 & 0 & \varepsilon_{33}^T \end{bmatrix} \begin{bmatrix} E_1 \\ E_2 \\ E_3 \end{bmatrix} \tag{5}$$

$$\begin{bmatrix} S_{11} \\ S_{22} \\ S_{33} \\ 2S_{23} \\ 2S_{13} \\ 2S_{12} \end{bmatrix} = \begin{bmatrix} S_{11}^E & S_{12}^E & S_{13}^E & 0 & 0 & 0 \\ S_{12}^E & S_{11}^E & S_{13}^E & 0 & 0 & 0 \\ S_{13}^E & S_{13}^E & S_{33}^E & 0 & 0 & 0 \\ 0 & 0 & 0 & S_{55}^E & 0 & 0 \\ 0 & 0 & 0 & 0 & S_{55}^E & 0 \\ 0 & 0 & 0 & 0 & 0 & 2\left(S_{11}^E - S_{12}^E\right) \end{bmatrix} \begin{bmatrix} T_{11} \\ T_{22} \\ T_{33} \\ T_{23} \\ T_{13} \\ T_{12} \end{bmatrix} + \begin{bmatrix} 0 & 0 & d_{31} \\ 0 & 0 & d_{31} \\ 0 & 0 & d_{33} \\ 0 & d_{15} & 0 \\ d_{15} & 0 & 0 \\ 0 & 0 & 0 \end{bmatrix} \begin{bmatrix} E_1 \\ E_2 \\ E_3 \end{bmatrix} \tag{6}$$

A huge variety of piezoelectric materials exist—well known are barium titanate ($BaTiO_3$) and lead zirconate titanate ($Pb(Zr, Ti)O_3$), known as PZT, as well as more flexible materials like polyvinylidene fluoride (PVDF). Most common are PWAS, made of PZT. They are separated into hard and soft PZTs by their coercive field. Hard PZTs exhibit a large linear drive region, showing small strain magnitudes and a relatively high Curie point ($T_C \approx 250^\circ$C); soft PZTs exhibit larger induced strain, while having a smaller linear region. Most soft PZTs have a Curie point above 150°C, but below those of hard PZTs. Examples of soft PZTs are PIC255, PSI 5A4E —Navy Type II, PIC151, PIC155, PZT5A-3195STD and PSI-5H4E Navy Type VI; examples for hard PZTs are PIC 181 and PIC 300, depending on the manufacturers naming (e.g., PICeramic, Piezo systems Inc.). In [21], a threshold of E_c =1 kV/mm to divide those two groups is mentioned.

For AU-based SHM systems, the use of PZT discs has proven to be useful. Different types of transducers exist. The simple form is a piezoceramic disc with a wrap-around electrode, which enables the soldering of both contacts on the top surface of the transducer, see **Figure 1a**. Alternatively, one might use PZT discs, which are already capsulated in embedding material. Depending on the application, the connecting cables are also embedded as conducting paths within a layer of embedding material. Examples are Acellent SMART layer© and DuraAct

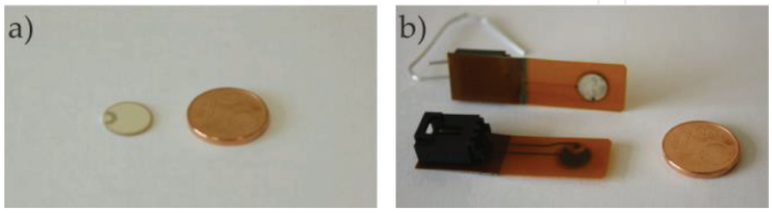

Figure 1. Types of transducers, (a) single transducer with wrap-around electrode from PICeramic, (b) embedded transducer, Acellent SMART layer©.

from PICeramic (see **Figure 1b**). Within this chapter, the first type is named single transducer/PWAS, while the second type is called embedded transducer/PWAS.

The generated wave field depends on the excitation frequency and the orientation of the transducer itself. In [22] it is shown that the orientation of the wrap-around electrode has significant influence on the generated wave field.

The use of PWAS for AU purposes has been described in a multitude of publications. An excellent overview is given in [21]. Herein, the interested reader will also find an extensive description of the governing equations for AU and EMI. In this chapter, only main results are cited.

For free disc-shaped transducers, the model is based on axial symmetry, leading to uniform radial and circumferential expansion. Using Eqs. (1) and (2) in cylindrical coordinates, the derivation of the induced strain and displacement—used for AU—as well as the electrical displacement, finally leading to the EMI spectrum, can be derived. As soon as the PWAS is attached to the structure, stress-free boundary conditions have to be replaced by a force equilibrium at the PWAS edges. Moreover, a shear layer coupling between PWAS and structure, achieved by the adhesive layer, needs to be considered. Based on [21, 23], in [4], a model was developed, which includes these effects and focuses on the PWAS signature, including resonances and antiresonances of the EMI spectrum $Z(\omega)$.

$$Z(\omega) = \left(i\omega C \left(1 - k_p^2 \left(1 - \frac{(1+\nu_a) J_1(\varphi_a)}{\varphi_a J_0(\varphi_a) - (1-\nu_a) J_1(\varphi_a) + \chi(\omega)(1+\nu_a) J_1(\varphi_a)} \right) \right) \right)^{-1} \tag{7}$$

It includes the Bessel functions of the first kind J, Poisson's ratio of the PWAS's material ν_a, the capacitance C, the coupling factor k_p, the frequency dependent stiffness quotient $\chi(\omega)$ and the abbreviation φ_a which can be derived by

$$C = \varepsilon_{33} \frac{\pi r_{pwas}^2}{h_{pwas}} \tag{8}$$

$$k_p^2 = \frac{2 d_{31}^2}{\varepsilon_{33} s_{11}^E (1-\nu_a)} \tag{9}$$

$$\varphi_a = \frac{\omega}{c} r_{pwas} \tag{10}$$

$$\chi(\omega) = \frac{k_{str\&adh}}{k_{pwas}} \tag{11}$$

When including the frequency dependent stiffness of the adhesive layer and a simple model for the stiffness of PWAS and structure, this can be included into $\chi(\omega)$.

$$k_{pwas} = \frac{h_{pwas}}{r_{pwas} s_{11}^E (1-\nu_a)} \tag{12}$$

$$\mathrm{k_{str\&adh}} = \frac{1}{\frac{1}{k_{str}} + \frac{1}{k_{adh}}} \tag{13}$$

$$k_{str} = \frac{2h_{str}E_{str}}{r_{pwas}(1-\nu_{str}^2)} \tag{14}$$

$$k_{adh} = \frac{G_{adh}}{2}\frac{\left(\frac{\omega}{c\sqrt{\alpha}}\right)^2}{\sinh^2\left(\frac{\omega h_{adh}}{c\sqrt{\alpha}}\right)}\left(\frac{\sinh\left(\frac{\omega h_{adh}}{c\sqrt{\alpha}}\right)}{2\frac{\omega}{c\sqrt{\alpha}}}+h_{adh}\right)\cdot\frac{1}{2}\frac{\frac{\omega}{c}r_{pwas}J_0^2\left(\frac{\omega}{c}r_{pwas}\right)^2-2J_0\left(\frac{\omega}{c}r_{pwas}\right)J_1\left(\frac{\omega}{c}r_{pwas}\right)+J_1^2\left(\frac{\omega}{c}r_{pwas}\right)}{\frac{\omega}{c}J_1^2\left(\frac{\omega}{c}r_{pwas}\right)} \tag{15}$$

This includes the geometry parameters $r_{PWAS}, h_{PWAS}, h_{str}, h_{adh}$, the material parameters elastic modulus E_{str}, Poisson's ratio ν_{str} and the wave speed for axially symmetric radial motion in the PWAS c.

It must also be kept in mind that many of the parameters used have complex values as damping has to be taken into account, e.g., $s_{11}^E = \widehat{s}_{11}^E(1-i\eta)$.

The frequency dependency of the characteristic structural stiffness was neglected. This model is therefore useful for analyzing the PWAS itself and its bonding condition, while it cannot be used for the modeling of changes respecting damages within the structure.

From Eq. (7), the susceptance B as the imaginary part of the admittance which is the inversion of the impedance can be calculated.

$$Y(\omega) = \frac{1}{Z(\omega)} \tag{16}$$

$$\mathrm{B}(\omega) = \mathrm{Im}\{\mathrm{Y}(\omega)\} \tag{17}$$

If neglecting the factor multiplied with k_p^2, the simple model of a PWAS as a capacitor gets visible. The capacitance C describes the slope, when plotting B over ω. This line is interrupted by the effects of the PWAS eigenfrequencies and its coupling with the structure. As the model does not include the frequency dependency of the structures stiffness, the peaks of eigenfrequencies of the stiffness are not visible. Other models include this frequency dependency of the structures stiffness, see [21]. Due to the necessary simplicity of these models, the applicability for SHM based on the EMI spectrum is limited, but they lead to a better understanding of its characteristic features.

3. Classification of transducer faults

Different types of PWAS faults result from different causes. Due to the continuous or periodical monitoring with permanently installed sensors, PWAS used for SHM need to be tested against degradation issues. Nevertheless, early faults within the PWAS service life have to be taken into account. Production deficiencies can lead to an insufficient bonding quality between structure and PWAS before the PWAS can be used for the first time. Depending on the type of fault, the effects on the generated wave field as well as on the EMI spectrum differ.

3.1. Cracks

When describing the fault type crack within this chapter, this refers to macro-size cracks. Different causes can lead to these cracks. During production or later use, falling objects, which hit the transducer itself, cause cracks and spalling. Two examples of single transducers impacted twice by falling mass (m = 53.5 g, h = 350 mm for (a), 450 mm for (b)) are shown in **Figure 2**.

Due to the nonsymmetric characteristic of the fault, the effects on the wave field are also nonsymmetric. **Figure 3** shows the signal, recorded by two neighboring transducers (PWAS 1 and PWAS 3), generated by a cracked PWAS (PWAS 2). The two signals differ significantly, showing the nonsymmetric characteristic of the fault. Single transducers as well as embedded transducers show decreased output when being cracked. The effect of spalling is not present for embedded transducers, as the embedding material holds the separated parts together. If a PWAS inspection system does not indicate these faults, the SHM system is based on corrupted signals and will most likely give alarm, although not the structure but the PWAS is damaged.

The effects of this type of fault on the EMI spectrum differ significantly depending on the type of transducer, see **Figure 4**. Due to the changed stiffness of the cracked PWAS, the resonance frequency changes. These changes are larger for the single transducers, while the effect is

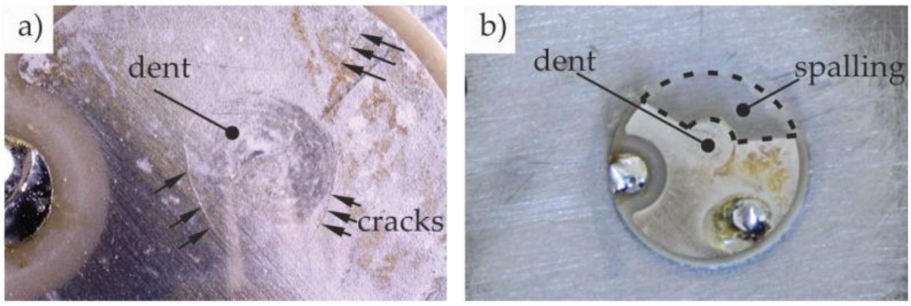

Figure 2. Micrographs of transducer fault type, (a) crack (b) crack and spalling.

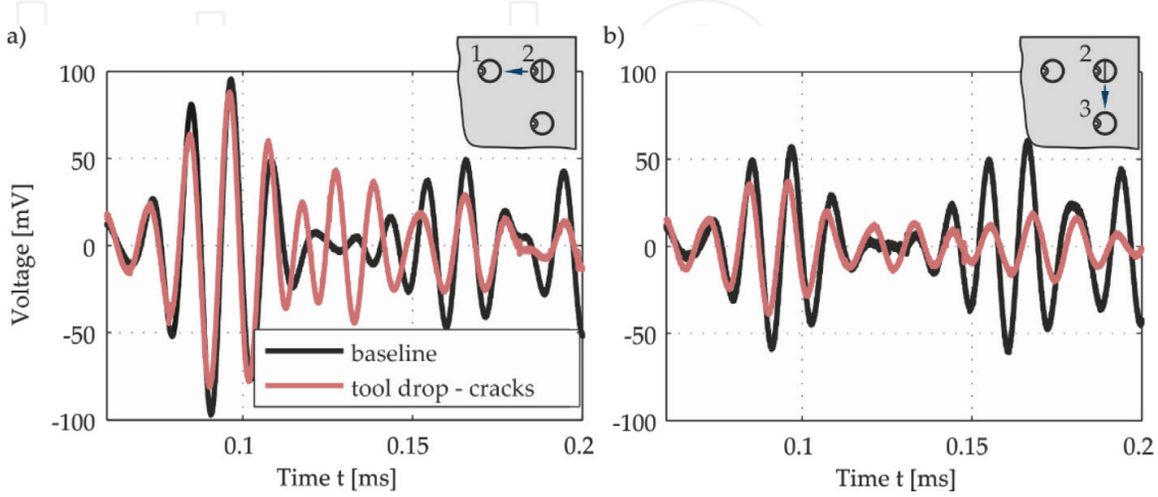

Figure 3. Change of wave propagation depending on the orientation of damage, (a) PWAS2-PWAS1, (b) PWAS2-PWAS3.

http://dx.doi.org/10.5772/intechopen.77298

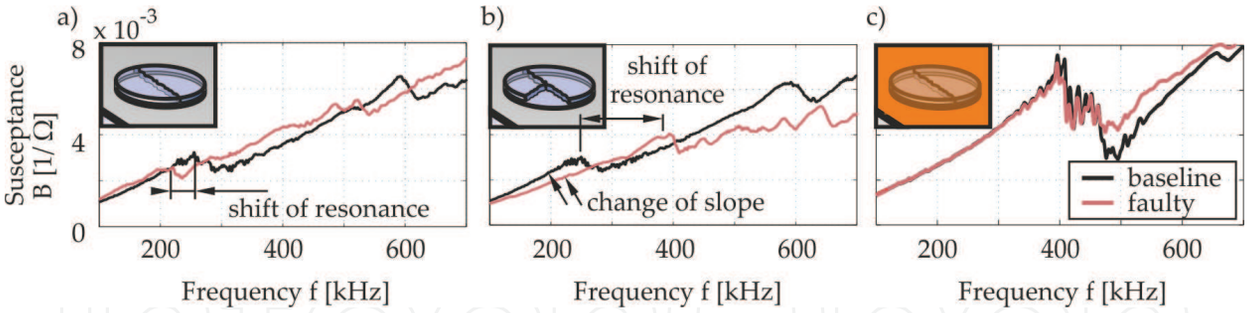

Figure 4. Change of EMI spectra depending on PWAS type and type of fault, (a) single transducer with crack, (b) single transducer with crack and spalling, (c) embedded transducer with crack.

decreased for the embedded transducers, where the embedding material leads to remaining stiffness between the cracked parts. A drop of capacitance, which will lead to a decreased susceptance slope is visible for the case of spalling. As the capacitance is proportional to the area, the reason for this drop is the missing piece of transducer, which is only the case for single transducers.

3.2. Degradation

Degradation of the piezoelectric transducer and its bonding to the structure is a major transducer fault especially for long-term monitoring, favored in structural health monitoring. It can be caused, e.g., by elevated temperatures. Depending on the selected adhesive (e.g., Hysol EA9394 by Henkel, Z70 by HBM) and the chosen PWAS material (e.g., PIC 255, PIC 151), either the adhesive or the piezoelectric material is prone to degrade. It has been shown in [24] that the pure exposure to outdoor conditions can also lead to minor degradation, which is visible in the generated wave field by a slightly decreased signal. Its level decreases uniformly. In **Figure 5**, the degradation, caused by elevated temperature, is shown.

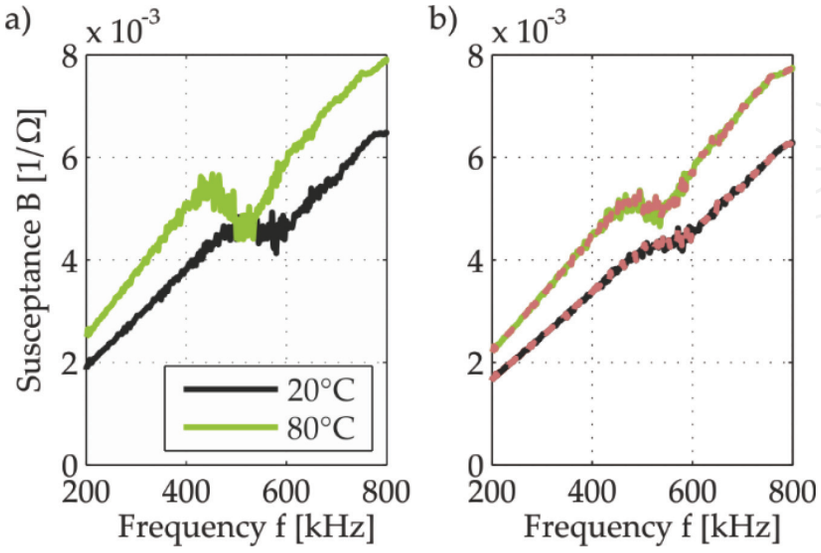

Figure 5. EMI spectra for 20 and 80°C, (a) baseline and (b) degraded state.

It led to a slight decrease of the susceptance slope, which is not caused by a change of the surface area but the degrading of the PWAS material and a change of its adhesive stiffness, see Eq. (15). If the temperature is unknown, degradation might be interpreted as temperature change.

3.3. Debonding

Debonding is a fault type, located at the adhesive zone between PWAS and structure. While a contaminated surface of the structure during the bonding process will lead to deficiencies of the bonding quality and debonding effects right from the beginning, fatigue of the bonding layer, e.g., under bending moments, might also lead to a debonding of the PWAS from the structure. The latter has a defined orientation of the fault, while a contamination might be local or evenly distributed over the bonding area. **Figure 6** shows the maxima of the out-of-plane component of the velocity field of a perfectly bonded transducer compared to the fields, generated by two PWAS, which were bonded on an aluminum plate, being contaminated with wax before bonding.

The out-of-plane velocity has been measured on the structure, from the back-site of the plate using a Laser Doppler Vibrometer CLV1000 with CLV700 head. The generated wave field of the debonded transducers is far from being symmetric and the generated amplitudes are smaller, compared to the perfectly attached transducer.

The debonding due to bending has been modeled by partial bonding of a PWAS to an aluminum plate. **Figure 7** shows the out-of-plane velocity, measured at the surface of the PWAS itself and from the back-site. A vibration of the debonded section is visible in **Figure 7a**. This energy is stored and transferred to the structure with a delay. The amplitude on the back is decreased in the debonded area.

The partial debonding also changes the frequency characteristic of a bonded PWAS. It has been shown that with some frequencies used as input frequency, the amplitudes, measured at a distance of 20 mm to the PWAS center, are larger for the debonded case; see **Figure 8**.

The debonding also leads to a changed EMI spectrum, the effects depend on the severity of debonding. **Figure 9** shows the effect of a 20% debonded surface, with four different orientations of the debonded area, relative to the wrap-around electrode.

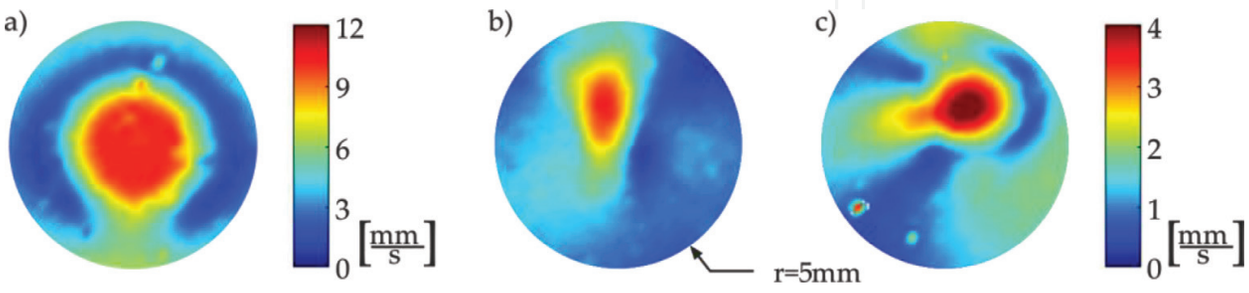

Figure 6. Maximum values of the out-of-plane velocity time signal, generated by the PWAS and transferred to the structure, measured by a laser vibrometer at the back of the structure, (a) perfectly attached PWAS, (b), (c) two PWAS attached on a plate with wax-contaminated surface.

http://dx.doi.org/10.5772/intechopen.77298

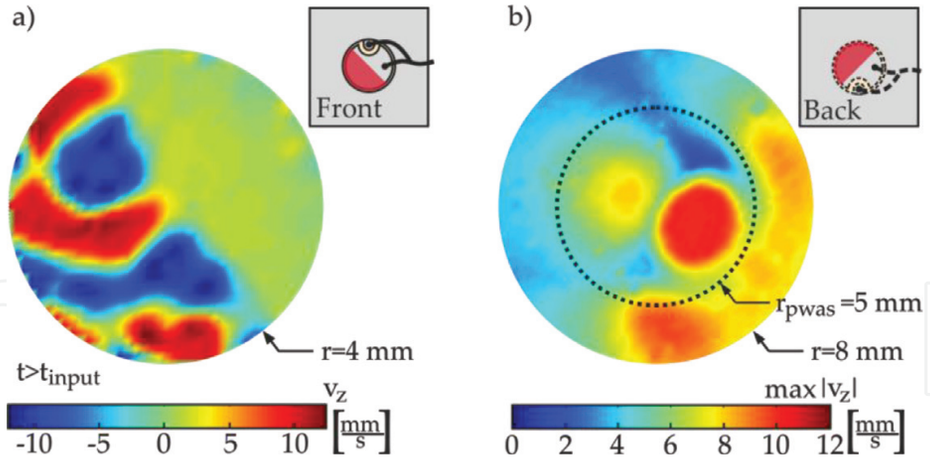

Figure 7. Out-of-plane velocity of a debonded PWAS, (a) measured at the top surface of the PWAS after the decay of the input signal, the radius of the circular measurement area is 4 mm, (b) measured at the back of the plate, the maxima of out-of-plane velocity are plotted, the dotted circle marks the PWAS location, the radius of the circular measurement area is 8 mm.

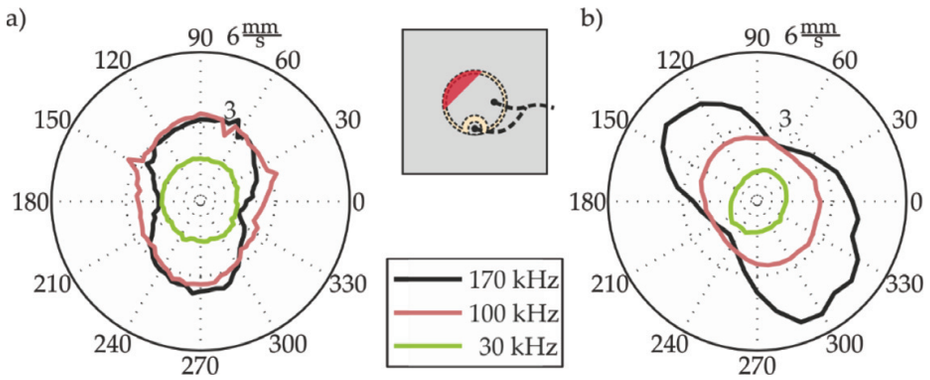

Figure 8. Maximum out-of-plane velocity at different angles for 30 kHz, 100 kHz and 170 kHz, measured at 20 mm distance, (a) for the fully bonded PWAS, (b) for the partially debonded PWAS.

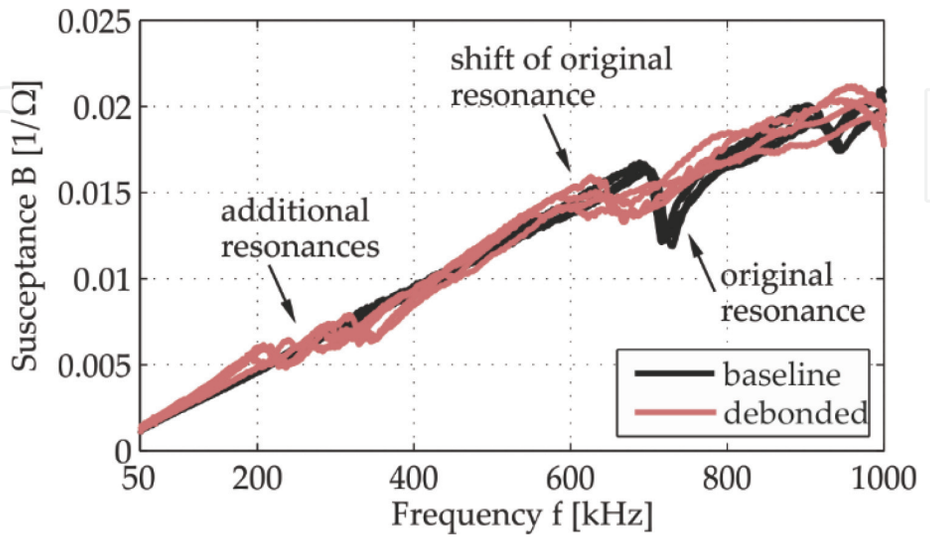

Figure 9. Effects of 20% debonded area on the susceptance spectrum. Four completely bonded PWAS are compared with four partially debonded PWAS. The orientation of the bonding relative to the wrap-around electrode has been changed.

4. Methods of transducer inspection

To achieve an increased reliability of SHM systems, a check of the systems' piezoelectric transducers and a good knowledge about the component itself is necessary. Refs. [24–28] pay attention to durability and long-term integrity as well as investigations on typical damage patterns. These investigations include stereomicroscopy [26], monitoring a possible change of the slope of electric charge over strain [26–28] and near-field scanning interferometry [24]. These methods are useful under laboratory conditions but cannot be transferred to the inspection of transducers during their employment and operation.

In [29], a method of transducer inspection based on a time reversal index, a symmetry index and a Lamb wave energy ratio index is suggested. Herein, the capacitance is used as a first indicator to finally separate structural damage, changes of environmental conditions and PWAS faults. The systems are partially based on analytical and hardware redundancy.

Using a second, independent measurement quantity, the EMI spectrum was discussed as a side issue in [30, 31] and later is focused in [32, 33]. They concentrate on the susceptance slope, which is increased by debonding and decreased if the PWAS breaks. As it can be seen in **Figure 4**, this is possible for some fault types and severe damages but does not detect, e.g., minor cracks and central debonding [34]. Further work in this regard can be found in [29, 35–39]. Using more information like the resonance behavior included in the EMI-spectrum enables the detection of minor PWAS faults and is especially valuable for the inspection of embedded transducers [40–42]. This is possible with the use of a physical model [4] or by utilizing purely data-driven approaches [43]. A simplified measurement of the EMI spectrum suggested in [44] and implemented, e.g., in [45] enables a quick measurement of the EMI spectrum with the same equipment as used for AU-based SHM systems. Based on the results of a PWAS inspection system, in [46, 47], signal correction factors are suggested to enable the exploitation of the signals in case of minor damage.

Within this section, the most used and elevated methods of transducer inspection based on the EMI spectrum, resp. the susceptance spectrum, are described. They are categorized into data-based and model-based methods. If a method allows to waive the explicit use of the temperature information for temperature compensation, this will be highlighted.

4.1. Model-based methods

For the inspection of PWAS with model-based methods, the analytical model, introduced in Section 2 can be used. The idea is to adapt the model to the experimental data via fitting of the parameters. The fitted parameter vector is used to separate the healthy state. Using principal component analysis (PCA), they can be aggregated to a damage index DI_{model}. For details, the reader is referred to [4, 42].

An advantage of this method is the nonnecessity to include temperature information for the test in application, also if the influence of environmental conditions should be compensated. Nevertheless, during training, temperature information is necessary.

As already shown in Eqs. (7-17), the model itself includes a bunch of parameters. Although most of them cannot be changed due to damage (e.g., nominal radius of the PWAS), these parameters will have some variations resulting from different batches, different bonding procedures, and so on. Therefore, the model needs to be adapted to the experimental baseline first. With this updated model, the model-based transducer inspection procedure can start.

The major disadvantage of this procedure is the high correlation of the different parameters on the influence on the susceptance spectrum. The adaptation of the parameters is based on optimization procedures, which do not necessarily result in physically meaningful parameters. Moreover, the user needs to know a multitude of parameters about the applied PWAS before being able to use this method.

4.2. Data-based methods

The avail of the EMI spectrum started from using the susceptance slope coefficient SC as the damage indicator [33, 37, 39]. As the capacitance is a linear factor for the susceptance, it can be seen as an advanced alternative to solely measure the PWAS capacitance. It is measured in a frequency range up to a small share of the eigenfrequency, which interrupts the constant slope. Although it has been shown that not all faults can be detected with this method, it is a simple method, which can be applied easily, and which detects severe damages like fracture of the PWAS.

The employment of more information from the susceptance spectrum than only using the slope is also possible with data-based methods. In [48], 12 parameters, which can be extracted from the susceptance spectrum, have been listed. After extraction from the spectrum, they are used for PCA. The first principal component (PC) can be taken as damage indicator for degradation and breakage. While data-based models in general are less numerically expensive than model-based methods, one difficulty of this method is to extract the parameters, depending on the data quality.

The inclusion of more information of the spectrum is also possible by using the correlation coefficient and subtracting its absolute value from 1 to achieve a damage index. This way, no additional extraction of features is necessary.

$$DI_{CC} = 1 - |CC| \text{ with } CC = \frac{V_{12}}{\sqrt{V_{11}V_{22}}}, \tag{18}$$

V_{kl} being the entries within the covariance matrix V. The correlation coefficient CC is 1 for two susceptance spectra, which only differ by a proportional change This way, the slope is an insensitive parameter for this method. Nevertheless, PWAS faults change the characteristic shape of the spectrum at resonance also for small faults. This is focused, when using the damage index based on the correlation coefficient DI_{CC}.

4.3. Transducer inspection in the context of the whole SHM system reliability

The quality of the inspection methods has to be assured not only by checking if specific damaged can be found; Moreover, the combination of SHM system and transducer inspection

needs to be checked. This is especially the case as most operators of SHM systems are not able to define specific types of transducer defects and its sizes to assess the quality of performance of a transducer inspection method. It therefore has to be ensured that the transducer inspection will find a faulty PWAS, before the signal deterioration will lead to a changed output of the SHM system. The authors emphasize that it is necessary to consider the algorithm of the SHM system as well as the PWAS inspection method to assess its performance. This way it is also possible to reconsider if data of a degraded transducer might still be used or has to be neglected.

A possible approach for this is described in [49, 42] and suggests using statistical methods, based on the probability of detection (POD) approach: it enables increased knowledge of the combination of transducer inspection and SHM system, including the value, which the structural damage detection indicator reaches, before a defective transducer can be detected with a probability of 90% at a confidence level of 95% (SDI_90|95). A complete reliability analysis needs to incorporate the interaction of SHM system and transducer inspection system.

5. Application scenarios

In this section, several application scenarios, including a comparison of different methods of transducer inspection, as described in Sections 4.1 and 4.2, are presented. Moreover, the results of these methods have to be evaluated taking into account the effects of the different defects of the results of the SHM system, which is implemented, as discussed in Section 4.3.

5.1. Detection of cracks in and debonding of transducers

To detect cracks and debondings, two data-based methods are compared in the following application scenarios. The most proposed method to inspect piezoelectric transducers is the monitoring of the susceptance slope. This is compared with the correlation coefficient-based method.

Cracks in an embedded transducer, bonded in central position on a CFRP strip, have been caused by four-point-bending of the strip (see **Figure 10a**) left down. First cracks started on reaching a strain level of 0.5%.

The EMI spectrum was always measured at unloaded condition after deforming the specimen at the following strain levels: 0.15, 0.3, 0.45, 0.5, 0.6, and 0.7%. **Figure 10b** shows that the multiple cracks of the embedded transducer after 0.7% strain led to a slight decrease of the susceptance slope, while the first two fault levels exhibit similar behavior like the undamaged states. For the correlation coefficient-based method, all three stages of fault can be clearly identified and separated from the undamaged state (see **Figure 10c**). For detailed information about the experimental setup, see [43, 42].

The debonding scenario is achieved by preventing the contact between adhesive and PWAS at approximately 20% of the surface area. This area was covered with Teflon tape during the process of gluing. Four different orientations of the debonded area relative to the wrap-around electrode have been tested (**Figure 11**).

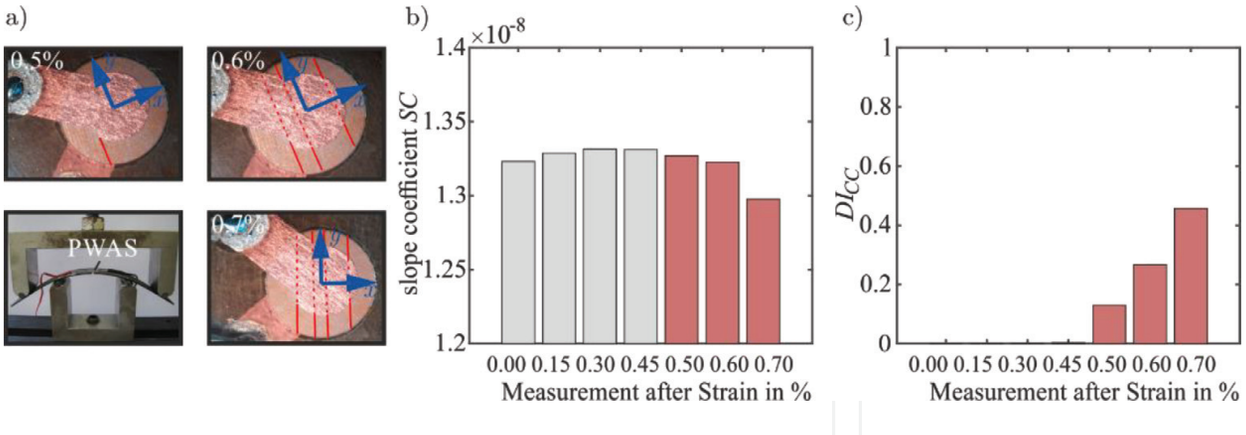

Figure 10. (a) Experimental setup with a four-point-bending test and micrographs of the three different crack states of an embedded DuraAct transducer caused by different strain levels (0.5, 0.6 and 0.7%), (b) slope coefficient *SC* of the impedance spectrum, (c) correlation coefficient-based damage index DI_{CC}, evaluated for measurements of four uncracked and three cracked states.

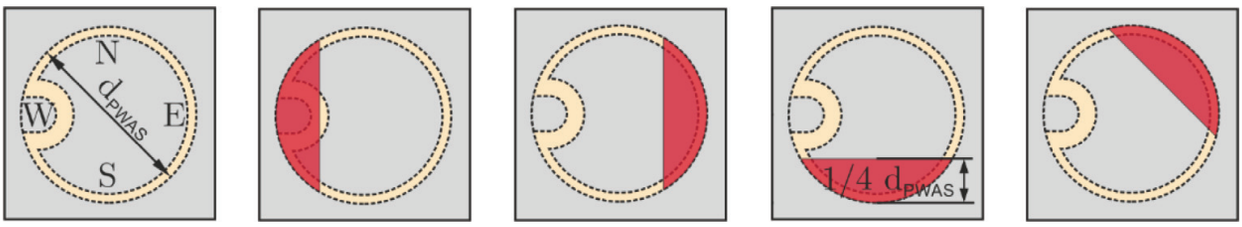

Figure 11. Debonding scenario and orientation of debonded area relative to the wrap-around electrode.

As this procedure makes it difficult to have a baseline measurement of each sensor, four fully bonded transducers are used as a baseline. For all eight transducers, the EMI spectrum has been recorded five times within an interval of 10 m. **Figure 12** shows the resulting damage indices.

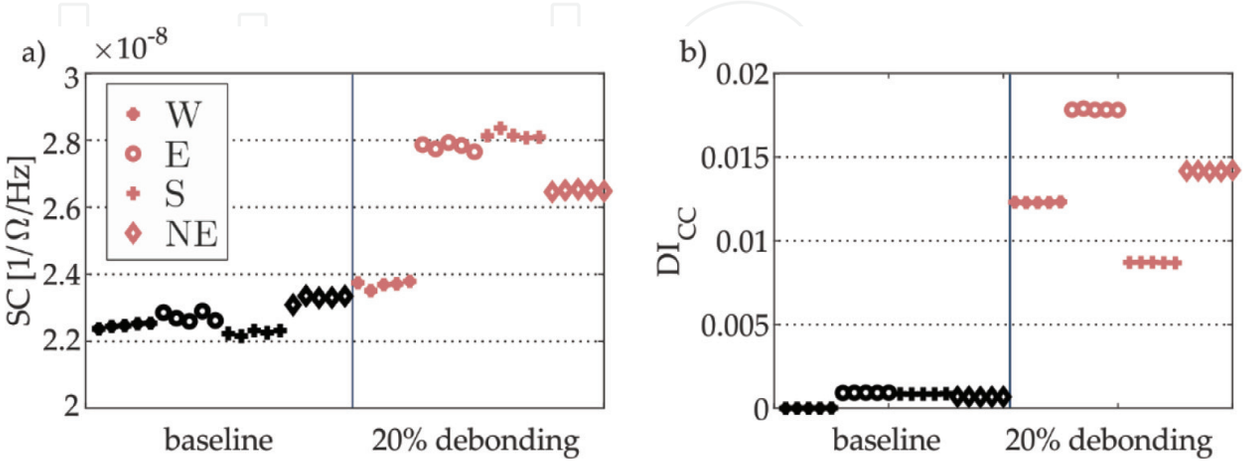

Figure 12. (a) Slope coefficient SC, (b) correlation coefficient-based damage indicator DI_{CC} for four fully bonded and four partially debonded transducers.

While the slope coefficient values are not normalized with a reference value, the reference for the correlation coefficient-based method is the first measurement of the first transducer. Using the slope coefficient, the difference between debonded and healthy state is small, especially for the debonding beneath the wrap-around electrode. For the correlation coefficient-based method, the debonding can be clearly separated from the fully bonded state. Moreover, the variation between the measurements of the same state is higher for the slope coefficient.

An analysis of the resulting wave propagation for these debonded PWAS can be found in [50]. For detailed information about the experimental setup and other debonding levels, see [42].

5.2. Inspection of transducers after system setup

The difficulty of transducer inspection after system setup is the absence of a proper reference. In many cases, this can be overcome with the help of a model-based approach. Nevertheless, in this application, a whole batch of transducers as a reference within the batch is used. Building the mean correlation coefficient for all combinations of all transducers, except a single one, and subtracting the mean correlation coefficient of all transducers with the single one from this value, this can be used as an indicator for the similarity of the single one with the whole batch. Another procedure without using a reference is described in [37], the use of correlation blocks is suggested in [14].

In this application, 16 transducers have been mounted on a plate structure. The plate has been contaminated with wax at two positions so that PWAS 12 and 16 are insufficiently bonded. Using the correlation coefficients of all combinations, the two contaminated PWAS could be clearly identified, see **Figure 13**, showing significantly higher indicator values than the rest of the sensors.

5.3. Inspection of transducers under changing temperature conditions

The influence of environmental and operational conditions is known to be nonnegligible for the automated continuous monitoring of structures in general. The effect on the inspection of piezoelectric transducers using the EMI spectrum therefore needs to be considered. In this

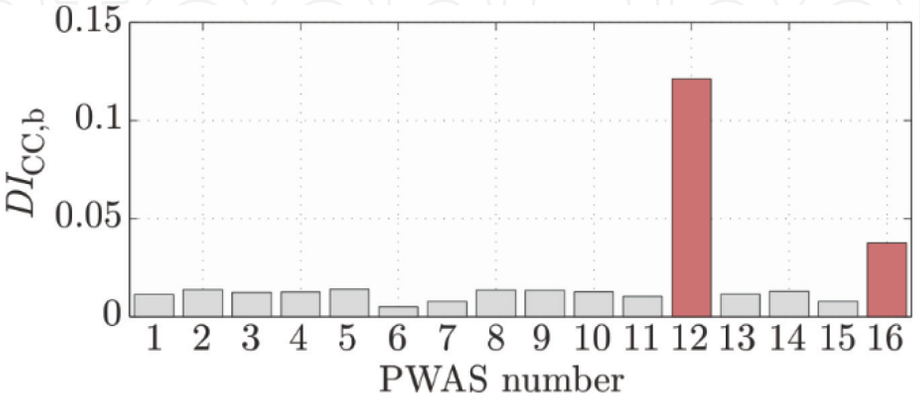

Figure 13. Damage indices, based on the comparison of correlation coefficients for all 16 PWAS after system setup. PWAS 12 and 16 are insufficiently bonded due to contamination with wax.

http://dx.doi.org/10.5772/intechopen.77298

application scenario, a model-based and a purely data-based method are used for the detection of degradation faults within a temperature range of 20–85°C.

As defect, a degradation of the adhesive as well as of the piezoelectric material was introduced to a PWAS by heat exposure for 32 h at 130°C. Fourteen measurements, equally distributed over the whole temperature range, have been used as reference data for the data-based approach to train the model for the model-based approach. Twenty-six measurements distributed over the whole temperature range are used as test data and 42 measurements over the whole temperature range have been recorded after degradation took place.

Figure 14 shows the results for the model- and data-based methods in (b) and (c) as well as the temperature present during the specific EMI measurement in (a).

Both methods clearly distinguish between the degraded and the healthy state. The results show that the model fits best for medium temperatures, although the whole temperature range was used for training. The model-based approach allows to waive the explicit use of the

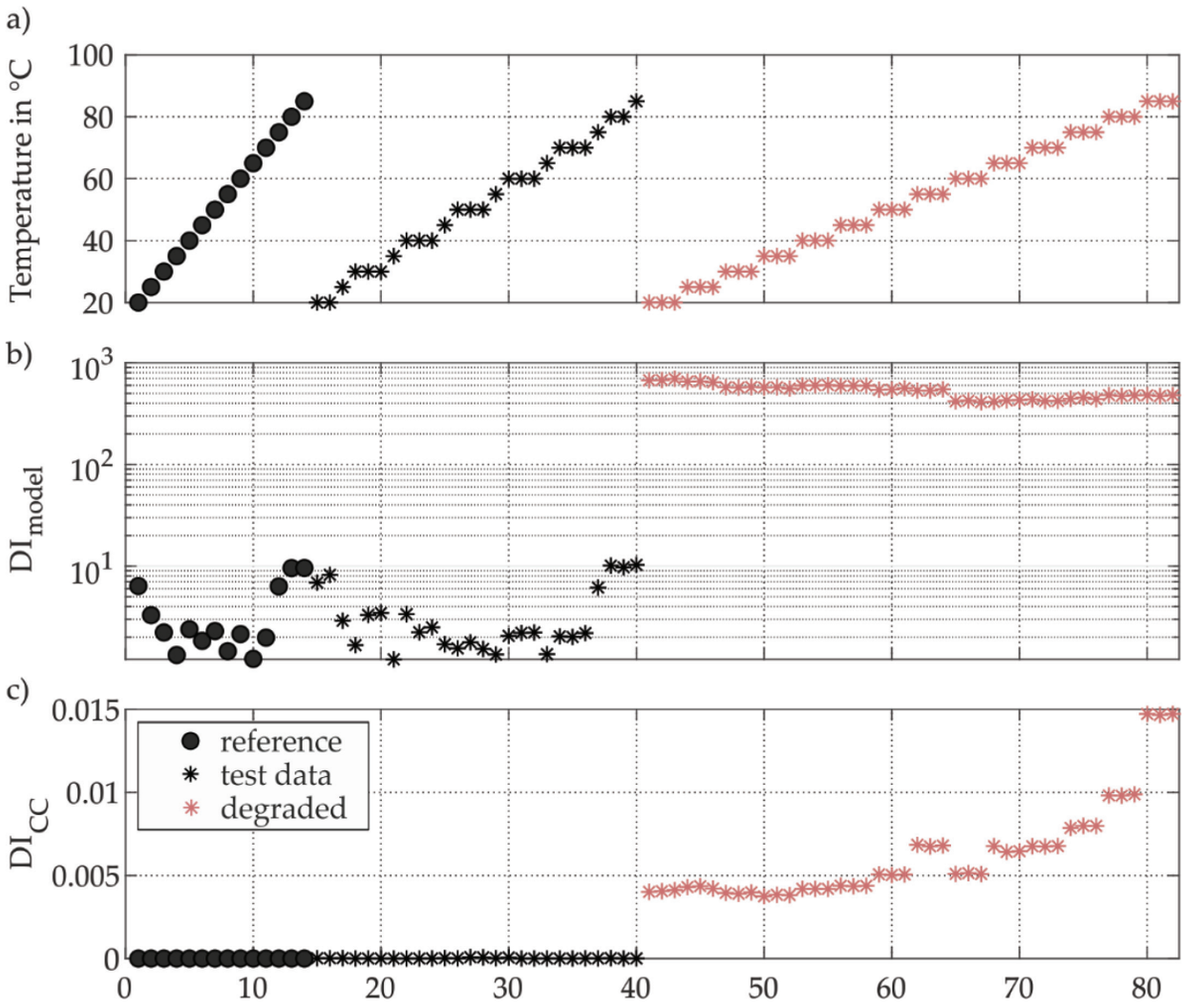

Figure 14. (a) Temperature, (b) DI_{model} and (c) DI_{CC} for several measurements of a single transducer before and after degradation of adhesive and piezoelectric material.

temperature information after the training is completed. The data-based approach employing the correlation coefficient needs the temperature information to select the correct baseline. For more information on the experimental setup and the estimated model parameters, see [4], on the data-based method, see [42].

6. Conclusion

Piezoelectric transducers are used within several SHM systems for a multitude of applications. For the system reliability, the proper functionality of the permanently installed transducers must be secured. This chapter proposes a system self-check, similar to other measurement equipment. For its realization, a detailed analysis of possible fault types and their effects on the generated wave field and the EMI spectrum is necessary. Moreover, it is tremendously important to incorporate the effects of possible PWAS faults on the SHM system to know if a faulty transducer will be identified before it will have an influence on the SHM system output and a false alarm will be produced. To enable the reader to increase the reliability of SHM systems, within this chapter several methods for transducer inspection have been presented. Their usage was demonstrated for different applications, showing disadvantages and advantages of the different methods. While model-based methods are linked to the necessity of an expert knowledge about the transducer and its bonding conditions, data-based approaches, using the correlation coefficient, need a temperature measurement to incorporate temperature changes. Especially for small cracks without spalling, using more aspects of the EMI than just the susceptance slope is advantageous.

Acknowledgements

Most of this work has been conducted during 2012–2016 within the framework of national and international cooperation, leading to the PhD thesis [42]. The authors would like to acknowledge Maria Moix-Bonet (DLR) and Martin Bach (Airbus), who have been a great help in identifying the need of research within this area and supported the research with samples and fruitful discussions especially regarding the damage types of degradation and crack. Moreover, the authors would like to acknowledge Alisa Shpak and Mikhail Golub from Kuban State University, Krasnodar, Russia, with whom they have worked on the modeling of the debonding fault and its experimental validation within the last years and enjoyed fruitful discussions.

Parts of this work are based on research activities within the EU 7th framework project SARISTU under grant agreement No. 284562 which is thankfully acknowledged.

Conflict of interest

The authors declare no conflict of interest. The founding sponsors and employers had no role in the design of the study; in the collection, analyses, or interpretation of data; in the writing of the manuscript and in the decision to publish the results.

Author details

Inka Mueller[1]* and Claus-Peter Fritzen[2]

*Address all correspondence to: inka.mueller@rub.de

1 Institute for Structural Engineering, Ruhr-Universität Bochum, Germany

2 Institute for Mechanics and Control Engineering—Mechatronics, University of Siegen, Germany

References

[1] Farrar CR, Worden K. Structural Health Monitoring: A Machine Learning Perspective. Chichester, West Sussex, United Kingdom: John Wiley & Sons Ltd; 2012

[2] Michaels JE, Michaels TE. Detection of structural damage from the local temporal coherence of diffuse ultrasonic signals. IEEE Transactions on Ultrasonics, Ferroelectrics and Frequency Control. 2005;**52**:1769-1782

[3] Baptista FG, Vieira Filho J, Inman DJ. Real-time multi-sensors measurement system with temperature effects compensation for impedance-based structural health monitoring. Structural Health Monitoring-an International Journal. 2012;**11**:173-186

[4] Buethe I, Eckstein B, Fritzen CP. Model-based detection of sensor faults under changing temperature conditions. Structural Health Monitoring. 2014;**13**:109-119

[5] Roy S, Lonkar K, Janapati V, Chang FK. A novel physics-based temperature compensation model for structural health monitoring using ultrasonic guided waves. Structural Health Monitoring. 2014;**13**:321-342

[6] Sohn H, Worden K, Farrar CR. Statistical damage classification under changing environmental and operational conditions. Journal of Intelligent Material Systems and Structures. 2002;**13**(9):561-574

[7] Figueiredo E, Park G, Farrar CR, Worden K, Figueiras J. Machine learning algorithms for damage detection under operational and environmental variability. Structural Health Monitoring-an International Journal. 2011;**10**:559-572

[8] Fritzen C-P, Kraemer P, Buethe I. Vibration-based damage detection under changing environmental and operational conditions. Advances in Science and Technology. 2013;**83**: 95-104

[9] Sepehry N, Shamshirsaz M, Abdollahi F. Temperature variation effect compensation in impedance-based structural health monitoring using neural networks. Journal of Intelligent Material Systems and Structures. 2011;**22**:1975-1982

[10] Buethe I, Kraemer P, Fritzen C-P. Applications of self-organizing maps in structural health monitoring. Key Engineering Materials. 2012;**518**:37-46

[11] PI Ceramic GmbH. https://www.piceramic.com/en/products/piezoceramic-components/

[12] Acellent Technologies Inc. http://www.acellent.com/en/products/sensors/

[13] Kullaa J. Detection, identification and quantification of sensor fault. In: Proceedings of ISMA 2010 Including USD2010; 2010

[14] Dunia R, Qin SJ, Edgar TF, McAvoy TJ. Identification of faulty sensors using principal component analysis. AICHE Journal. 1996;**42**:2797-2812

[15] Guo S, Zhong Z, He T. FIND: Faulty node detection for wireless sensor networks. In: Proceedings of the 7th ACM Conference on Embedded Networked Sensor Systems, New York, NY, USA; 2009

[16] Friswell MI, Inman DJ. Sensor validation for smart structures. Journal of Intelligent Material Systems and Structures. 1999;**10**:973-982

[17] Worden K. Sensor validation and correction using auto-associative neural networks and principal component analysis. In: IMAC-XXI: Conference and Exposition on Structural Dynamics; Orlando, USA. 2003

[18] Kraemer P, Fritzen C-P. Sensor fault identification using autoregressive models and the mutual information concept. Damage Assessment of Structures VII. 2007;**347**:387-392

[19] Reimann P, Dausend A, Schutze A. A self-monitoring and self-diagnosis strategy for semiconductor gas sensor systems. IEEE Sensors. 2008;192-195

[20] Köppe E, Bartholmai M, Daum W, Gong X, Holmann D, Basedau F, Schukar V, Westphal A, Sahre M, Beck U. New self-diagnostic fiber optical sensor technique for structural health monitoring. Materials Today: Proceedings. 2016;**3**:1009-1013

[21] Giurgiutiu V. Structural Health Monitoring: With Piezoelectric Wafer Active Sensors. Oxford (Academic Press): Elsevier Science; 2007

[22] Moll J, Golub MV, Glushkov E, Glushkova N, Fritzen C-P. Non-axisymmetric lamb wave excitation by piezoelectric wafer active sensors. Sensors and Actuators A-Physical. 2012; **174**:173-180

[23] Dugnani R. Dynamic behavior of structure-mounted disk-shape piezoelectric sensors including the adhesive layer. Journal of Intelligent Material Systems and Structures. 2009; **20**:1553-1564

[24] Blackshire JL, Giurgiutiu V, Cooney A, Doane J. Characterization of Sensor Performance and Durability for Structural Health Monitoring Systems. In: proceedings of SPIE's 12th International Symposium on Smart Structures and Materials. San Diego, CA. March 2005

[25] Blackshire S, Cooney A. Characterization and Modeling of Bonded Piezoelectric Sensor Performance and Durability in Simulated Aircraft Environments. 2006

[26] Gall M, Thielicke B, Schmidt I. Integrity of piezoceramic patch transducers under cyclic loading at different temperatures. Smart Materials and Structures. 2009;**18**:104009

[27] Gall M. Experimentelle und numerische Untersuchungen zur Lebensdauer von flächigen ppiezokeramische Sensor-/Aktor – Modulen [PhD thesis]; 2012

[28] Bach M, Dobmann M, Eckstein B, Moix-Bonet M, Stolz M. Reliability of co-bonded piezoelectric sensors on CFRP structures. In: 9th International Workshop on Structural Health Monitoring; 2013

[29] Lee SJ, Sohn H, Hong JW. Time reversal based piezoelectric transducer self-diagnosis under varying temperature. Journal of Nondestructive Evaluation. 2010;**29**:75-91

[30] Giurgiutiu V, Zagrai A, Bao JJ. Piezoelectric wafer embedded active sensors for aging aircraft structural health monitoring. Structural Health Monitoring. 2002;**1**:41-61

[31] Pacou D, Pernice M, Dupont M, Osmont D. Study of the interaction between bonded piezo-electric devices and plates. In: 1st European Workshop on Structural Health Monitoring; 2002

[32] Park G, Farrar CR, Rutherford AC, Robertson AN. Piezoelectric active sensor self-diagnostics using electrical admittance measurements. Journal of Vibration and Acoustics. 2006;**128**: 469-476

[33] Park G, Farrar CR, Scalea FL, Coccia S. Performance assessment and validation of piezoelectric active-sensors in structural health monitoring. Smart Materials & Structures. 2006; **15**:1673-1683

[34] Rugina C, Enciu D, Tudose M. Numerical and experimental study of circular disc electromechanical impedance spectroscopy signature changes due to structural damage and sensor degradation. Structural Health Monitoring. 2015;**14**:663-681

[35] Bach M, Fritzen B, Eckstein B, Speckmann H. Self-diagnostic capabilities of piezoelectric transducers using the electromechanical impedance. In: International Workshop of Structural Health Monitoring; 2007

[36] Park S, C-BY, Inman DJ. Structural health monitoring using electro-mechanical impedance sensors. Fatigue & Fracture of Engineering Materials & Structures. 2008;**31**:714-724

[37] Overly TG, Park G, Farinholt KM, Farrar CR. Piezoelectric active-sensor diagnostics and validation using instantaneous baseline data. IEEE Sensors Journal. 2009;**9**(11): 1414-1421

[38] Lee SJ. Development of Smart Piezoelectric Transducer Self-Sensing, Self-Diagnosis and Tuning Schemes for Structural Health Monitoring Applications. Pittsburgh, Pennsylvania, USA: Carnegie Mellon University; 2009

[39] Taylor SG, Park G, Farinholt KM, Todd MD. Diagnostics for piezoelectric transducers under cyclic loads deployed for structural health monitoring applications. Smart Materials and Structures. 2013;**22**:025024

[40] Buethe I, Fritzen CP. Sensor performance assessment based on a physical model and impedance measurements. Key Engineering Materials. 2013;**570**:751-758

[41] Mueller I, Fritzen C-P. Inspection of piezoceramic transducers used for structural health monitoring. Materials. 2017;**10**(1):17

[42] Mueller I. Inspection of piezoelectric transducers used for structural health monitoring systems [PhD thesis]; 2016

[43] Buethe I, Moix-Bonet M, Wierach P, Fritzen CP. Check of piezoelectric transducers using the electro-mechanical impedance. In: EWSHM—7th European Workshop on Structural Health Monitoring, Nantes; 2014

[44] Overly TGS. Development and integration of hardware and software for active-sensors in structural health monitoring [MSc thesis]; 2007

[45] Fritzen CP, Moll J, Chaaban R, Eckstein B, Kraemer P, Klinkov M, Dietrich G, Yang C, Xing KJ, Buethe I. A multifunctional device for multi-channel EMI and guided wave propagation measurements with PWAS. In: EWSHM—7th European Workshop on Structural Health Monitoring, Nantes; 2014

[46] Mulligan KR, Quaegebeur N, Masson P, Brault L-P, Yang C. Compensation of piezoceramic bonding layer degradation for structural health monitoring. Structural Health Monitoring. 2014;**13**:68-81

[47] Masson P, Quaegebeur N, Mulligan K, Ostiguy PC. Increasing the roburobust in damage imagin for SHM. In: International Symposium on SHM and NDT; 2013

[48] Xing K. Experiments and simulation in structural health monitoring systems using the E/M impedance and cross transfer function methods [PhD thesis]; 2015

[49] Buethe I, Fritzen CP. Quality assessment for the EMI-based inspection of PWAS. In: International Workshop on Structural Health Monitoring, Stanford; 2015

[50] Golub MV, Shpak AN, Buethe I, Fritzen CP, Jung H, Moll J. Continuous wavelet transform application in diagnostics of piezoelectric wafer active sensors in Days on Diffraction; 2013